COMEC

The 10th International Conference on COMPUTATIONAL MECHANICS AND VIRTUAL ENGINEERING

Transilvania University of Brasov
FACULTY OF MECHANICAL ENGINEERING

25-27 October 2023

Ultrasound method for determination of porosity in Laser Additive-Manufactured Titanium alloy

Savin A.[1,2*], Stanciu M.D.[2], Prevorovsky Z.[3], Soare M.[4], Iftimie N[1]., Steigmann R.[1] and Nový F.[5]

1. NDT Department, National Institute of R&D for Technical Physics, Iasi, Romania
2. Faculty of Mechanical Engineering, Transilvania University of Brașov, Romania
3. Department of Impact and Waves in Solids, Institute of Thermomecanics, Prague, Czech Republic
4. Nuclear NDT Research & Service, Bucharest, Romania
5. Faculty of Mechanical Engineering, University of Žilina, Žilina, Slovak Republic

*Corresponding author: asavin@phys-iasi.ro

Abstract: Metal additive manufacturing are developing faster and faster, gaining in popularity, although they involve technological processes with variable parameters giving the performance and quality of the product. Metal laser powder bed fusion (L-PBF) are frequently used in the producing of Ti-6Al-4V parts for aerospace, electronics, biomedical, automotive applications, benefiting from the 3D design technology that ensures a broad vision of the appearance and structure of the final product. The paper presents the possibility of evaluating the integrity of AM parts from the analysis of C-scan ultrasonic images in amplitude or time of flight–and the correlation of the results with those obtained by optical microscopy and metallography. The methods allow emphasizing distribution of flaws as pores or voids in the volume, the detailing the flaws and location ensures the possibility of management review.

Keywords: *additive manufacturing, ultrasound testing, C-scan, microstructure*.

1. INTRODUCTION

Additive manufacturing (AM) of metallic materials is considered a technology with future application potential in industry [1], based on the concept of 3D printing [2].The process based on metal laser powder bed fusion (L-PBF) developed specifically for printing metal alloys, use a laser source or an electron beam. L-PBF is one of the most common methods of making metal parts with complex geometries. Thus Ti-6Al-4V (Ti64) parts can be produced, adapted to the type of application, from medical components, mold and tools to complex geometry for industrial parts. L-PBF depends on the type of laser used, the laser power and the scanning mode for melting the powder, also the powders used require quality microstructural characteristics to not generate flaws [3]. These can affect surface roughness and the presence of voids and pores inside it. Roughness is an essential quality parameter for the automotive, aerospace and medical industries. Thus, consistent quality assurance (QA) of the product within

the limits prescribed by standards, costs and time remains a continuous concern. Permanent monitoring can ensure the detection of flaws in real time [4], the non-destructive evaluation of materials (NDE) based on conventional techniques [5,6], can provide potentially information which will ensure the profitability of the AM process and the transition to QA automatic learning[7].

The paper presents the result of the C-scan method using ultrasonic images in amplitude or time of flight to emphasize discontinuities of Ti64 samples realized by L-PBF technology.

2. Materials and methods

Titanium and its alloys, due lower density, associated with good mechanical properties, high corrosion resistance, is recommended at fabrication of light parts required in technological and industrial applications [8, 9]. Ti64 has good processing conditions, the stability of the microstructure can be obtained in the form of bars or plates. Bars Ti64 samples, having 59.50x9.40x14.49 mm^3, were made with AM-LPBF powder bed using grade 5 powder to avoid the occurrence of granulation leading to excessive porosities (ASTM F2924-14) [10], were provided by Institute of Thermomechanics, Prague, Czech Republic, Figure 1. Each sample has an artificial defect inside in the middle area, with disk shape, 5mm diameter and thickness of 0.2mm, 0.3mm, 0.4mm and 0.5mm.

Figure 1. Studied AM samples of Ti64.

These samples were used for metallographic analyzes and for C-scan ultrasonic test. The software of the equipment can display the data in 2D format, allowing the analysis of the C scan images to identify defects or other discontinuities. Optical evaluations of the sample's surface were carried out as well as the analysis of the chemical composition, the obtained values fall within the ranges of values according to ASTM B348-09 [11] (Table 1).

Table 1. Ti64 chemical analysis results (wt.%).

Sample		**Al**		**V**		**Fe**	Ru,Cr,Ni,Cu, Nb,Zr,Sn,Pb	**Ti**
		trans	long	trans	long			
#1		5.78	5.40	4.26	4.30	0.26	<0.02	Bal.
#2		6.76	4.96	4.22	4.32	0.24		
#3		6.98	4.83	4.22	4.33	0.23		
#4		5.59	5.27	4.34	4.24	0.25		
Titanium Grade 5	min	5.50		3.50		-	-	-
B348-09	max	6.75		4.50		0.40	-	-
Incertitude		±0.27		± 0.12		± 0.05	-	-

Micorhardness tests were made in 5 random points using the Nemesis 9102-Innovatest equipment conform ISO 6506–1:2015 [12].

To analyze the microstructure of the surfaces, a chemical attack with a mixture of HF (20%), HNO_3 (10%), and water H_2O (70%) was carried out. The samples

were investigated using a Zeiss AXIO Observer Z1m metallographic microscope. The C-scan ultrasonic testing (ISO/ASTM TR 52905:2023)[13] is applicable to AM samples to detect porosity [14] or the quality of metal components, detect defects and highlight the microstructure. C-scan renders the image US examination results, showing a cross-section of the tested object parallel to the scanned surface by combining measurements obtained over the entire thickness of the sample. The image is made from the data collected from the US inspection and represented on a plan view of the component. The equipment used in the C-scan ultrasonic testing is Nuclear MicroSonic - Mark IV owned by Nuclear NDT Research & Service Ltd. The equipment consists in a fluid tank, a controller of the mechanical displacement, (X, Y, Z, θ), US emission-reception system, data acquisition board and a PC. It has been shown that C-scan imaging is the best method for identifying and visualizing the results, allowing the mapping of flaws in the samples, by projecting the US data on a plan view of the tested area, displaying an image. For C-scan analysis, the transducer sweeps the surface of the samples placed together along length parallel to X axis. Time of flight and normal beam back-echo methods are used.

3. Results

The data from the literature show that at AM LPBF, the prediction of porosity, which affects the mechanical performance of a product, takes on a major importance. Information about density and structure of the samples is obtained evaluating the microstructure. The Brinell hardness test for studied samples show values in the [314÷318]HB2.5/187.5 range, close despite the small difference of microstructure. Figure 2 presents the microscopies of the samples after chemical attack confirming the stability of parameters during the printing through good densification and without major flaws.

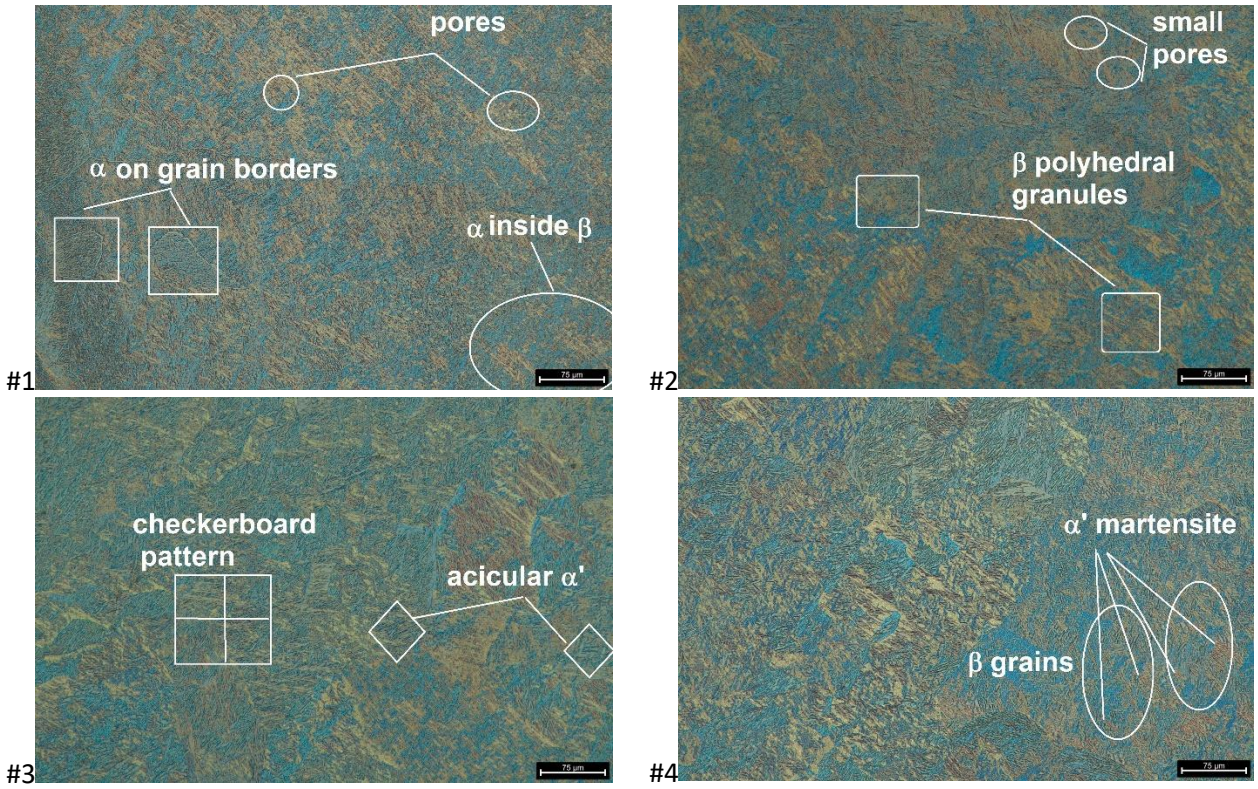

Figure 2 Metallography of studied samples, 75X magnification

Figure 2 presents the microscopies of the samples after chemical attack which confirm the stability of parameters during the samples printing through good densification and without major flaws. The pores in sample #1 and #2 are small. Also, #2 presents polyhedral granules, #3 fine grains, #4 has particles dispersed in α in the grain's borders and lamellas of α' inside the β phase grains. These are primary grains in β phase due to exceeding the deposition temperature of Ti64 [15, 16]. The most common NDE method for all materials is ultrasonic testing, the frequency of received ultrasonic waves ranging between 1 and 15 MHz. C-scan technique use a focused transducer with high sensitivity to detect pores with dimensions <1mm. Metallographic analysis of Ti64 showed low porosity, so to cause sufficient attenuation variation, an US transducer with smaller beam focal diameter is required for high sensitivity. The ultrasonic C-scan images were obtained with focused point transducer of 15 MHz, with effective diameter of 0.25" and focal distance length of 2". Fine mineral oil was used as coupling to prevent any possible corrosion and superficial oxidation. US velocity was 4380m/s and it has been used to calculate the depth of the flaws. Ultrasonic dimensions and depth of flaws are given in the Table 2.

Table 2. US results.

Sample	Samples Dimensions [mm]	Ultrasonic Diameter of Flaws [mm× mm]	Ultrasonic Flaws Depth [mm]
#1	59.42x9.40x14.47	2.8 × 3.6	8.1 ÷ 8.3
#2	59.50x9.34x14.38	3.2 × 4.0	8.6 ÷ 9.0
#3	59.34x9.31x14.47	3.2 × 3.8	8.6 ÷ 9.0
#4	59.37x9.28x14.49	3.6 × 4.8	8.1 ÷ 8.6

The interval of minimal and maximal values of flaw's depth are based on the fact that surface of flaws is not perfect, thus US reflections on surface gave multiple echoes.

There are significant differences with the intentional flaw's diameters (5 mm), as big as the flaws thickness is decreasing (from sample #4 to sample #1). The technique based on time-of-flight (TOF) monitors the time of the diffracted signal from the upper surface of the defect and depends only on the depth of the defect. TOF can be used during scanning with normal beam as well as angle beam pitch-catch-scan. The C scan back-wall echo images of the AM samples are presented in Figure 3. C-scan shows data obtained in amplitude of wave or depth (time of flight).

The percentage of the amplitude and time of flight results from the ratio between the individual values measured into an acquisition point and the maximum values allowed by the equipment on the respective channels. Depth information can be obtained by using TOF methods, indicated by different color shadings.

During the scanning, the samples were placed next to each other, Figure 3 a with exposed surface and the length parallel to the X axis. The incidence of the ultrasonic normal beam was normal of exposed surface. From the amplitude analysis obtained from the internal defects in samples #1 to #4, it can be seen that they are placed at the same depth below the subsurface and allows the estimation of the dimensions of the defects in the circumferential-axial plane.

Figures 3a and b are based on amplitude and TOF of the Back Echo and c is based on TOF of Flaw Echo. The characteristics of the defects were observed

(they slipped inside the sample), therefore the circular shape of the defects (figure 3a) is no longer respected.

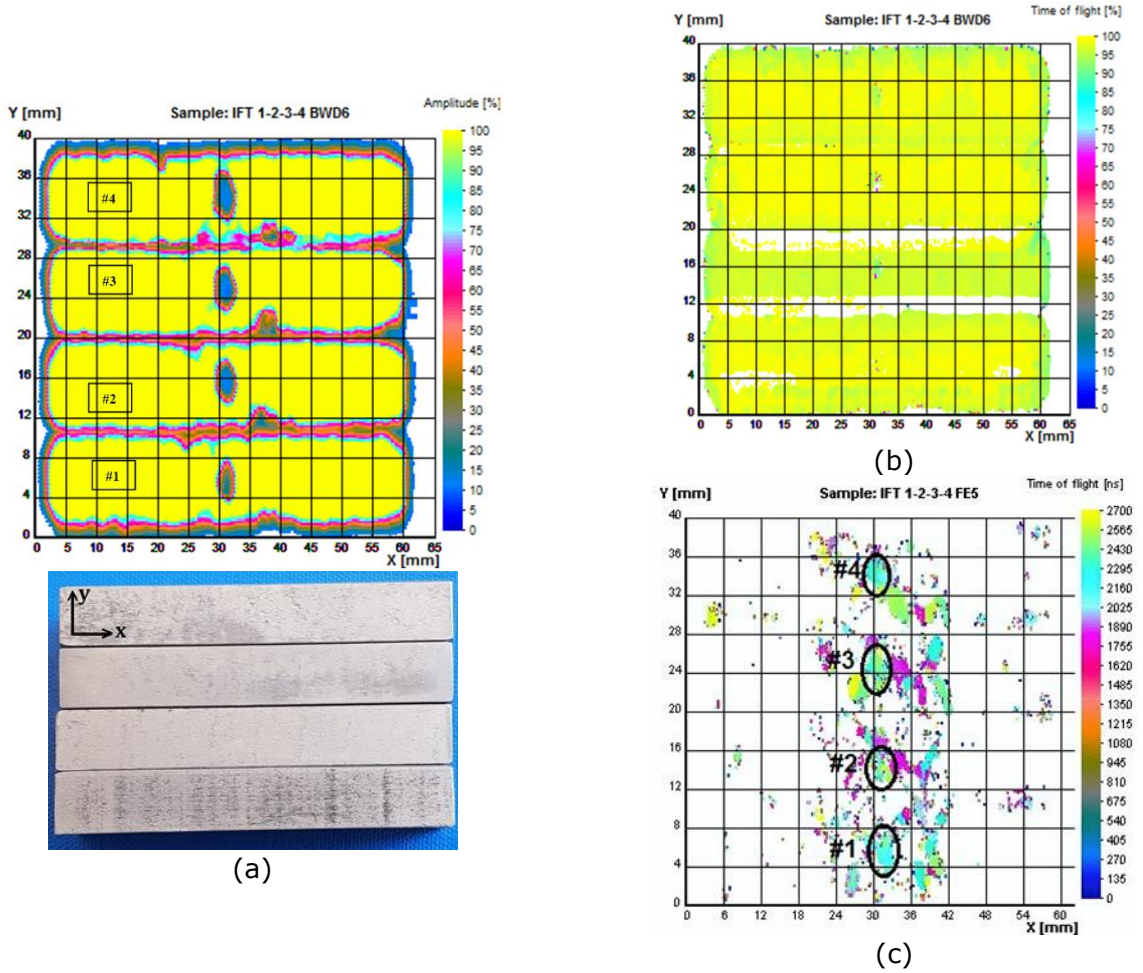

Figure 3: Ultrasonic testing of Samples 1 to 4: (a) amplitude image, examination ISA-FE5 on Back Echo; (b) Time of flight image, examination ISA-FE5 of Back Echo.; c) examination ISA-FE5 on Flaw Echo, used for determination of flaw depth in respect to the surface of incidence.

The errors/uncertainties are determined especially by possible inhomogeneities of acoustic-elastic properties leading to variations of propagation velocities and of reflection coefficients /reflectivity of discontinuities. The transducer sweeps the surface of the samples placed next to each other, with the length parallel to the X axis. The method used is time of flight as well as normal beam back-echo. In the case of the flaw echo (figure 3c) the spectral properties of the defect diameter are more complex. Similar to grain noise, Flaw Echo can be modeled as a convolution between the impact ultrasonic pulse and the impulse response function of the defect, taking into account the effect of frequency-dependent attenuation. Thus, the effect of backscattering the acoustic energy (which determines the main echo, selected on the gate) overlaps with the effect of mode conversion at the surface of the defect (which determines the secondary echo, which does not intervene) in the spectral analysis. However, it is important to note that the spectral domains of the two signals (back and flaw echo respectively) are distinct: the high frequency area for the flaw echo and, respectively, the low frequency area for the back echo in the presence of the defect.

4. Conclusions

C-scan method using ultrasonic images in amplitude or time of flight can emphasize discontinuities of Ti64 samples realized by laser powder bed fusion (L-PBF) technology. The types and pattern of flaws can be identified by single mapping, removing the inspection errors. It has the ability to monitor and visualize the volumetric flaws reducing the inspection and analysis time, leading to increasing of quality and reliability. US method can be applied as complementary NDE to improve the precision and optimize AM process.

Acknowledgements

This work was supported by the Romanian Ministry of Research, Innovation and Digitization, under Nucleus Program, Project PN 23-11 and Program1—Development of the National R&D system—Contract PFE 5/2021., as well as CNCS/CCCDI—UEFISCDI, project number 61PCE/2022, PN-III-P4-PCE2021-0885, ACADIA.

References

[1] Delic M., Eyers, D.R. The effect of additive manufacturing adoption on supply chain flexibility and performance: An empirical analysis from the automotive industry. Int. J. Prod. Econ. 2020, 228, 107689
[2] Jadhav A. and Jadhav V.S., 2022. A review on 3D printing: An additive manufacturing technology. Materials Today: Proceedings, 62, pp.2094-2099.
[3] Zhou L.Y., Fu J. and He Y., 2020. A review of 3D printing technologies for soft polymer materials. Advanced Functional Materials, 30(28), p.2000187.
[4] Zahidin M.R., et al. Research challenges, quality control and monitoring strategy for Wire Arc Additive Manufacturing. J. Mater. Res. Technol., 24, 2769–2794, 2023.
[5] Fritsch T. et al. 3D computed tomography quantifies the dependence of bulk porosity, surface roughness, and re-entrant features on build angle in additively manufactured IN625 lattice struts. Advanced Engineering Materials., 24, 6, 2022.
[6] Ehlers H., Pelkner M., & Thewes R. Heterodyne eddy current testing using magnetoresistive sensors for additive manufacturing purposes. IEEE Sensors Journal, 20(11), 5793–5800, 2020.
[7] Herzog T., Brandt M., Trinchi A., Sola A. and Molotnikov A., Process monitoring and machine learning for defect detection in laser-based metal additive manufacturing. Journal of Intelligent Manufacturing, pp.1-31. 2023.
[8] Donachie, M.J., Titanium: a technical guide. ASM international. Eds 2, 2000.
[9] Srinivasu G.S. and Raja N.R., Finite Element Modeling of Stress Strain Curve and Micro Stress and Micro Strain Distributions of Titanium Alloys—A Review. Journal of Minerals and Materials Characterization and Engineering, 11(10), p.953. 2012.
[10] ASTM F2924-14(2021) Standard Specification for Additive Manufacturing Titanium-6 Aluminum-4 Vanadium with Powder Bed Fusion
[11] ASTM B348-09 Standard Specification for Titanium and Titanium Alloy Bars and Billets
[12] ISO 6506-1:2014: Metallic materials — Brinell hardness test — Part 1: Test method
[13] ISO/ASTM TR 52905:2023(en) Additive manufacturing of metals — Non-destructive testing and evaluation — Defect detection in parts
[14] Hassen A.A., Kirka M.M. Additive Manufacturing: The rise of a technology and the need for quality control and in-spection techniques. Mater. Eval. 2018. 76(4), pp.438-453.
[15] Cao, S.; Zou, Y.; Lim, C.V.S. and Wu, X. Review of laser powder bed fusion (LPBF) fabricated Ti-6Al-4V: Process, post-process treatment, microstructure, and property. Light Adv. Manuf. 2021, 2(3), pp.313-332.
[16] Munk J., Breitbarth E., Siemer T., Pirch N. and Häfner C. Geometry Effect on Microstructure and Mechanical Properties in Laser Powder Bed Fusion of Ti-6Al-4V. Metals. 2022; 12(3): 482.